Quantum Reflection of He_2 Several Nanometers Above a Grating Surface

Bum Suk Zhao, *et al.*

Science **331**, 892 (2011);
DOI: 10.1126/science.1200911

illumination gives ~35% output. When the phase is adjusted to maximize the scattering, the output reaches ~70%.

Although we have demonstrated coherent reduction of absorption in our experiment, this effect should be distinguished from the phenomenon of electromagnetically induced transparency, in which absorption is suppressed by coherently driving the absorbing medium itself (*24*), instead of by enhancing escape from the cavity by constructive interference, as in our system.

Because this optical effect is easily realized in silicon, coherent perfect absorbers may enable novel functionalities in silicon integrated photonic circuits of the type envisioned for next-generation optical communications and computing applications (*25*) as well as for coherent laser spectroscopy. The simplest versions of the device immediately would serve as compact on-chip interferometers, which absorb or scatter the input beams instead of steering them. Although our current CPA operates near the silicon band edge, it should be possible to fabricate devices in which an additional parameter tunes the absorption coefficient independently of λ (e.g., by free carrier injection or by optical pumping), allowing one to fix the operating wavelength by design. Direct–band gap semiconductors also are suitable materials for CPAs, assuming that fluorescent emission can be tolerated or avoided in a specific application. Recent theoretical work has proposed a fascinating extension of the CPA concept, suitable for direct–band gap materials: Systems with balanced gain and loss can function simultaneously as a CPA and as a laser (i.e., as an interferometric amplifier-attenuator) (*26*, *27*). The CPA effect is not immediately applicable to photovoltaic or stealth technology because it is a narrow-band effect requiring coherent inputs.

More generally, the exact time-reversal symmetry property that relates laser emission to coherent perfect absorption implies that an arbitrarily complicated scattering system can be made to perfectly absorb at discrete frequencies if its imaginary refractive index can be tuned continuously over a reasonable range of values, and if appropriate coherent incident beams can be imposed. Progress in these areas would open up interesting new avenues for future research and applications.

References and Notes

1. E. L. Hahn, *Phys. Rev.* **80**, 580 (1950).
2. G. Bergmann, *Phys. Rep.* **107**, 1 (1984).
3. Y. Kuga, A. Ishimaru, *J. Opt. Soc. Am. A* **1**, 831 (1984).
4. M. P. Van Albada, A. Lagendijk, *Phys. Rev. Lett.* **55**, 2692 (1985).
5. P. E. Wolf, G. Maret, *Phys. Rev. Lett.* **55**, 2696 (1985).
6. C. H. Lewenkopf, H. A. Weidenmuller, *Ann. Phys.* **212**, 53 (1991).
7. M. Fink *et al.*, *Rep. Prog. Phys.* **63**, 1933 (2000).
8. J. de Rosny, M. Fink, *Phys. Rev. Lett.* **89**, 124301 (2002).
9. De Rosny and Fink (*8*) demonstrated a process of perfect absorption of time-reversed acoustic waves, but this requires a dynamic sink that is driven externally with appropriate amplitude and phase. This process is not related to time-reversed lasing.
10. G. Lerosey, J. de Rosny, A. Tourin, M. Fink, *Science* **315**, 1120 (2007).
11. Y. D. Chong, L. Ge, H. Cao, A. D. Stone, *Phys. Rev. Lett.* **105**, 053901 (2010).
12. See supporting material on *Science* Online.
13. A. E. Siegman, *Phys. Rev. A* **39**, 1253 (1989).
14. W. A. Hamel, J. P. Woerdman, *Phys. Rev. A* **40**, 2785 (1989).
15. R. H. Yan, R. J. Simes, L. A. Coldren, *IEEE Photon. Technol. Lett.* **1**, 273 (1989).
16. K.-K. Law, R. H. Yan, J. L. Merz, L. A. Coldren, *Appl. Phys. Lett.* **56**, 1886 (1990).
17. K.-K. Law, R. H. Yan, L. A. Coldren, J. L. Merz, *Appl. Phys. Lett.* **57**, 1345 (1990).
18. J. F. Heffernan, M. H. Moloney, J. Hegarty, J. S. Roberts, M. Whitehead, *Appl. Phys. Lett.* **58**, 2877 (1991).
19. K. Kishino *et al.*, *IEEE J. Quantum Electron.* **27**, 2025 (1991).
20. M. S. Ünlü, K. Kishino, H. J. Liaw, H. Morkoç, *J. Appl. Phys.* **71**, 4049 (1992).
21. M. Cai, O. Painter, K. J. Vahala, *Phys. Rev. Lett.* **85**, 74 (2000).
22. A. Yariv, *IEEE Photon. Technol. Lett.* **14**, 483 (2002).
23. J. R. Tischler, M. S. Bradley, V. Bulović, *Opt. Lett.* **31**, 2045 (2006).
24. S. E. Harris, *Phys. Today* **50**, 36 (1997).
25. M. Lipson, *J. Lightwave Technol.* **23**, 4222 (2005).
26. S. Longhi, *Phys. Rev. A* **82**, 031801(R) (2010).
27. Y. D. Chong, L. Ge, A. D. Stone, http://arxiv4.library.cornell.edu/abs/1008.5156v1 (2010).

28. Supported by NSF grants DMR-0808937 and DMR-0908437 and by seed funding from the Yale NSF-MRSEC (DMR-0520495). We thank E. Dufresne for use of his laser facility, and D. Miller and J. Bleuse for drawing our attention to the literature on asymmetric Fabry-Perot modulators and resonant cavity-enhanced photodetectors, respectively.

Supporting Online Material

www.sciencemag.org/cgi/content/full/331/6019/889/DC1
Materials and Methods
Figs. S1 and S2

22 November 2010; accepted 19 January 2011
10.1126/science.1200735

Quantum Reflection of He_2 Several Nanometers Above a Grating Surface

Bum Suk Zhao,* Gerard Meijer, Wieland Schöllkopf

Quantum reflection allows an atom or molecule to be reflected from a solid before it reaches the region where it would encounter the repulsive potential of the surface. We observed nondestructive scattering of the helium dimer (He_2), which has a binding energy of 10^{-7} electron volt, from a solid reflection grating. We scattered a beam containing the dimer as well as atomic helium and larger clusters, but could differentiate the dimer by its diffraction angle. Helium dimers are quantum reflected tens of nanometers above the surface, where the surface-induced forces are too weak to dissociate the fragile bond.

A neutral atom or molecule approaching a solid surface experiences an attractive force caused by the van der Waals atom-surface interaction potential, as sketched in Fig. 1A. In a classical picture, the particle accelerates toward the surface until it scatters back from the steep repulsive-potential branch. In quantum-mechanical scattering, a wave packet approaching the surface exhibits a nonvanishing reflection coefficient even when it is in the attractive part of the potential. Thus, despite the force acting toward the surface, there is some probability that the particle will reflect tens of nanometers or more above the surface, without ever colliding with the repulsive potential wall. The probability for this counterintuitive effect, termed quantum reflection, even approaches unity in the low-energy limit of the incident particle [e.g., (*1*)]. Quantum reflection from a solid was first observed by Shimizu for ultracold metastable Ne (*2*) and He (*3*) atoms. Later, it was also observed with helium atom beams (*4*, *5*). Here, we demonstrate that quantum reflection allows for nondestructive scattering of extremely fragile helium dimers from a ruled reflection grating.

The van der Waals–bound dimer of two ground-state helium atoms, He_2, is the most fragile ground-state molecule known (*6*, *7*). The binding energy of 10^{-7} eV leads to an exceptionally large bond length (mean internuclear distance) of 5.2 nm (*8*). The helium dimer is a quantum system because the probability for He_2 to be found in a classically forbidden state, where the internuclear separation is larger than the system's classical outer turning point, is more than 80% (Fig. 1B). Moreover, because rotational or vibrational excitation leads to dissociation, there are no excited bound states. These distinctive features have made He_2 an attractive model system for computational methods in quantum chemistry.

Trying to observe nondestructive scattering of He_2 from a solid surface appears to be an ill-conceived experiment. Even at grazing incidence, where the kinetic energy associated with the dimer's momentum component perpendicular to the surface can be smaller than the binding energy, the dimer is likely to be torn apart by the forces exerted on both atoms in the surface–potential-well region sketched in Fig. 1A. The potential-well depth is typically ~5 meV, hence,

Fritz-Haber-Institut der Max-Planck-Gesellschaft, Faradayweg 4-6, 14195 Berlin, Germany.

*To whom correspondence should be addressed. E-mail: zhao@fhi-berlin.mpg.de

four orders of magnitude larger than the dimer binding energy. Consequently, classical surface reflection of He_2 has not been observed in 80 years of He beam scattering since the first experiments by Stern and co-workers, who already used a ruled diffraction grating (*9*) as well as a crystal surface (*10*).

In our experiment, a collimated helium beam, containing atoms as well as small clusters, scatters under grazing incidence from a blazed diffraction grating (Fig. 1C). The orientation of the grating is such that its grooves are almost parallel to the plane spanned by the incident and specular beams. The diffraction experiment takes advantage of the atoms and clusters in the beam having the same mean velocity. Thus, the de Broglie wavelengths and, hence, the diffraction angles are inversely proportional to the particle mass, thereby leading to separate diffraction peaks of atoms, dimers, and larger clusters (*7*).

Figure 2A shows a diffraction pattern for P_0 = 1 bar measured with the detector, an electron-impact ionization mass spectrometer, set to a mass of 4 atomic mass units (amu). At this ion-mass channel, not only atoms but also clusters can be detected, because the latter can fragment upon electron impact, thereby releasing a He^+ ion. From its diffraction angle, the small peak between the intense specular and first-order diffraction peak of the monomer is identified as the first-order diffraction peak of the dimer. Another measurement for identical conditions, but with the detector set to the 8-amu ion-mass channel, is shown in Fig. 2B. At this channel the monomer peaks are absent, and the dimer peaks are expected to be weak because the probability for a dimer to not fragment upon electron-impact ionization is just a few percent (*11*). In addition to a specular peak, a diffraction peak is again seen at the calculated dimer diffraction angle, thereby confirming the peak assignments.

To confirm that the peaks attributed to dimers are not due to other clusters, we took measurements for various stagnation pressures. A diffrac-

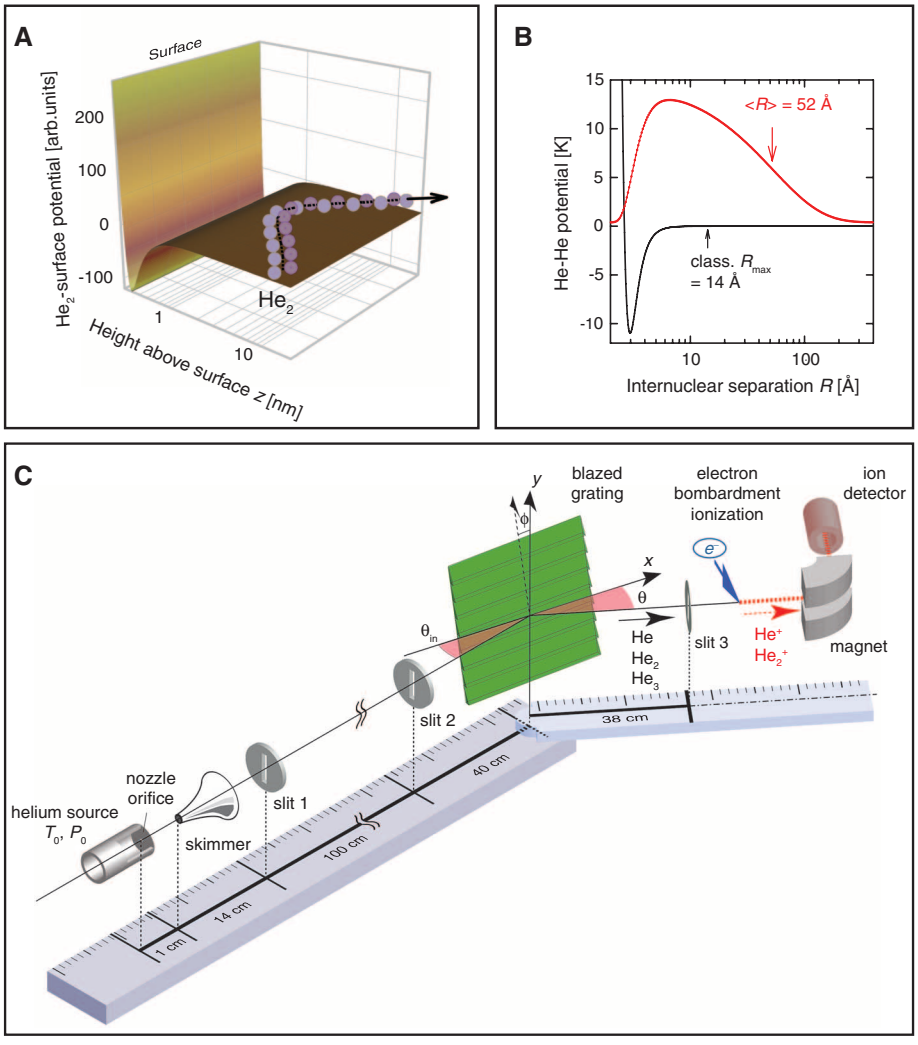

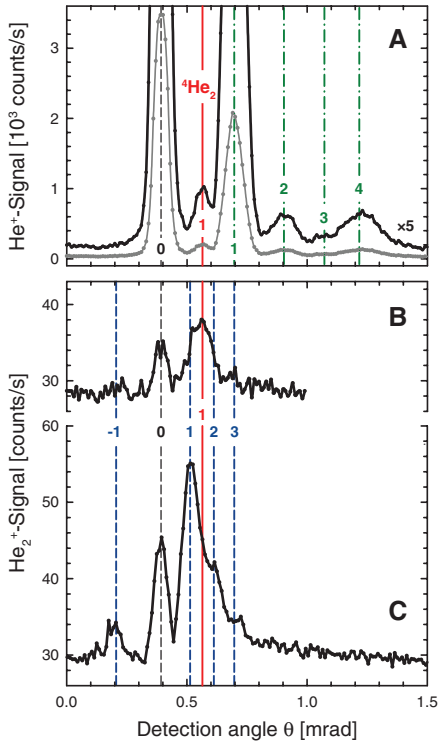

Fig. 1. (**A**) Artist's view of quantum reflection of a helium dimer at the attractive van der Waals surface potential. (**B**) The He-He interaction potential (*13*) (black) and the calculated probability function of $^4He_2$ (red) as a function of internuclear separation. (**C**) Schematic of the experimental setup. The continuous helium beam is formed by free-jet expansion of pure ^{4}He gas at a stagnation temperature T_0 = 8.7 K and pressure P_0 = 1 to 2 bar through a 5-μm-diameter orifice into vacuum. In the adiabatic expansion, the gas rapidly cools down to a temperature of ~1 mK, where weakly bound dimers and trimers are formed (*12*). The mean beam velocity of 300 m/s corresponds to de Broglie wavelengths (λ) of He, He_2, and He_3 of 3.32, 1.66, and 1.11 Å, respectively. At an incidence angle θ_{in} = 0.39 mrad, the grating-surface normal component of the velocity is 0.12 m/s. This corresponds to a kinetic energy of He_2 along the surface normal of only 0.57 neV. Here the incidence angle and the detection angle θ are measured with respect to the grating surface plane. The plane ruled blazed grating (Newport 20RG050-600-1) is made out of 6-mm-thick glass with an aluminum coating and has a surface area of 5 cm by 5 cm. It is characterized by a period d = 20 μm and a blaze angle of 14 mrad. The azimuthal orientation of the grating is set to ϕ = 10 mrad. High angular resolution of about 0.12 mrad is achieved by two 20-μm-wide collimation slits upstream of the grating in combination with a 25-μm-wide detector entrance slit. The nth-order diffraction angle θ_n follows from the grating equation $\cos\theta_{in} - \cos\theta_n = n\,(\lambda/d)\sin\phi$.

Fig. 2. Diffraction patterns of helium beams for two different stagnation pressures and measured with two different mass channels of the detector. (**A**) The 4-amu mass channel, P_0 = 1 bar. (The dark trace represents a fivefold magnification of the intensity.) (**B**) The 8-amu mass channel, P_0 = 1 bar. (**C**) The 8-amu mass channel, P_0 = 2 bar. At 4 amu (A), atoms and, due to fragmentation in the detector, also clusters can be detected, whereas at 8 amu (B and C) the atomic component of the beam is absent. The calculated diffraction angles of He, He_2, and He_3 are indicated by green dash-dotted, red solid, and blue dashed vertical lines, respectively, each labeled by the diffraction order number. The thin dashed black line indicates the 0th-order peak position.

tion pattern for $P_0 = 2$ bar recorded at a mass of 8 amu is shown in Fig. 2C. In this measurement, additional peaks are present, and their positions agree nicely with the calculated diffraction angles of the helium trimer. These findings are fully consistent with previous observations that more trimers are formed at increased stagnation pressure (*12*). In addition, it is known that trimers are more efficiently detected at a mass of 8 amu than dimers (*11*), further enhancing the trimer peaks relative to those of the dimer.

The observed nondestructive scattering of He_2 as well as He_3 from a reflection grating exemplifies the peculiar nature of a quantum-mechanical impact. Quantum reflection causes helium dimers and trimers to reflect tens of nanometers above the actual surface, where surface-induced forces are too feeble to break up even the fragile He_2 bond.

References and Notes

1. H. Friedrich, G. Jacoby, C. G. Meister, *Phys. Rev. A* **65**, 032902 (2002).
2. F. Shimizu, *Phys. Rev. Lett.* **86**, 987 (2001).
3. H. Oberst, Y. Tashiro, K. Shimizu, F. Shimizu, *Phys. Rev. A* **71**, 052901 (2005).
4. V. Druzhinina, M. DeKieviet, *Phys. Rev. Lett.* **91**, 193202 (2003).
5. B. S. Zhao, S. Schulz, S. Meek, G. Meijer, W. Schöllkopf, *Phys. Rev. A* **78**, 010902 (2008).
6. F. Luo, G. C. McBane, G. Kim, C. F. Giese, W. R. Gentry, *J. Chem. Phys.* **98**, 3564 (1993).
7. W. Schöllkopf, J. P. Toennies, *Science* **266**, 1345 (1994).
8. R. E. Grisenti *et al.*, *Phys. Rev. Lett.* **85**, 2284 (2000).
9. F. Knauer, O. Stern, *Z. Phys.* **53**, 779 (1929).
10. I. Estermann, O. Stern, *Z. Phys.* **61**, 95 (1930).
11. W. Schöllkopf, J. P. Toennies, *J. Chem. Phys.* **104**, 1155 (1996).
12. L. W. Bruch, W. Schöllkopf, J. P. Toennies, *J. Chem. Phys.* **117**, 1544 (2002).
13. K. T. Tang, J. P. Toennies, C. L. Yiu, *Phys. Rev. Lett.* **74**, 1546 (1995).

14. We thank J. R. Manson for insightful discussions. B.S.Z. acknowledges support by the Alexander von Humboldt Foundation and by the Korea Research Foundation Grant funded by the Korean Government (KRF-2005-214-C00188).

25 November 2010; accepted 12 January 2011
10.1126/science.1200911

Spin Selectivity in Electron Transmission Through Self-Assembled Monolayers of Double-Stranded DNA

B. Göhler,[1] V. Hamelbeck,[1] T. Z. Markus,[2] M. Kettner,[1] G. F. Hanne,[1] Z. Vager,[3] R. Naaman,[2]* H. Zacharias[1]

In electron-transfer processes, spin effects normally are seen either in magnetic materials or in systems containing heavy atoms that facilitate spin-orbit coupling. We report spin-selective transmission of electrons through self-assembled monolayers of double-stranded DNA on gold. By directly measuring the spin of the transmitted electrons with a Mott polarimeter, we found spin polarizations exceeding 60% at room temperature. The spin-polarized photoelectrons were observed even when the photoelectrons were generated with unpolarized light. The observed spin selectivity at room temperature was extremely high as compared with other known spin filters. The spin filtration efficiency depended on the length of the DNA in the monolayer and its organization.

Double-stranded DNA (dsDNA) is chiral both because of its primary structure and because of its secondary, double helix, structure. Owing to its broken mirror image symmetry, when a charge moves within a chiral system in one direction, it creates a magnetic field. The direction of spin polarization of photoelectrons emitted from nonmagnetic substrates, which exhibit high spin-orbit coupling, depends on the handedness of the circularly polarized light. Photoelectrons emitted from a bare gold substrate upon exposure to linearly polarized light would not be expected to show spin polarization. An organic chiral layer on a nonmagnetic metal surface is not expected to be self-magnetized, and photoelectrons ejected from such a layer with linearly polarized light would also be unpolarized. However, we observed exceptionally high polarization of electrons ejected from surfaces coated with a self-assembled monolayer of dsDNA, independent of the polarization of the incident light. By directly measuring the spin of the transmitted electrons with a Mott polarimeter, we found spin polarizations exceeding 60% at room temperature. This observation establishes the prospect of using dsDNA, or other chiral molecules, as a spin filter.

Unconventional magnetic properties affecting spin transport have been reported for inorganic-inorganic interfaces (*1*), topological insulators (*2*), graphene (*3*, *4*), and organic molecules adsorbed on magnetic substrates (*5*). Organic molecules would seem unlikely candidates for spin-selective transport properties because of their weak spin-orbit coupling. However, studies of photoelectrons ejected from gold surfaces covered with self-assembled, organized monolayers of chiral molecules show that the emission intensity depends on the circular polarization of the exciting light (*6*) as well as the voltage across the layer and its handedness (*7*, *8*). In these studies, the spin of the transmitted electron was not measured directly, and spin-dependent transmission was inferred from the dependence of the total electron transmission on the circular polarization of the incident photons. Furthermore, those studies could not directly determine whether the ejected electrons are highly polarized when the incident photons are unpolarized, or if the effect results simply from circular dichroism, namely, that the absorption of the system depends on the light circular polarization (*9*).

[1]Physikalisches Institut, Westfälische Wilhelms-Universität Münster, D-48149 Münster, Germany. [2]Department of Chemical Physics, Weizmann Institute, Rehovot 76100, Israel. [3]Department of Particle Physics and Astrophysics, Weizmann Institute, Rehovot 76100, Israel.

*To whom correspondence should be addressed. E-mail: ron.naaman@weizmann.ac.il

The sample preparation is similar to that described in (*10*). Self-assembled dsDNA monolayers are prepared according to standard procedures by depositing dsDNA, which is thiolated on the 3′ end of one of the DNA strands [see Supporting Online Material (*10*)] on a clean gold substrate (*11*) (Fig. 1). Four different lengths of dsDNA were investigated: 26, 40, 50, and 78 base pairs (bp) long. We used either polycrystalline Au or single-crystal Au(111) as substrates. The monolayers were characterized by various methods that ensure the uniformity and reproducibility of the DNA layer (*12*). The experiments were carried out under ultrahigh-vacuum conditions. Two photoelectron detection schemes were used: an electron time-of-flight instrument that recorded the kinetic energy distribution of the electrons and a Mott-type electron polarimeter for spin analysis (figs. S1 to S3). The photoelectrons were ejected by an ultraviolet (UV) laser pulse with photon energy of 5.84 eV, pulse duration of about 200 ps at 20-kHz repetition rate, and a fluence of 150 pJ/cm^2. The laser light was incident normal to the sample and was either linearly or circularly polarized. No damage was observed during the course of the spin polarization measurement (~4 hours).

For direct polarization measurements, the photoelectrons were guided by an electrostatic 90°-bender and subsequent transport optics. Hence, an initial longitudinal spin polarization is converted into a transverse one for analysis. In the electron polarimeter, an electron spin polarization causes a scattering asymmetry $A = (I_U - I_L)/(I_U + I_L)$. Here $I_{U,L}$ denotes the count rates in the upper and lower counter in the Mott polarimeter (fig. S1) (*13*, *14*). The transverse polarization is given by $P = A/S_{eff}$. The analyzing power, the Sherman function (*15*), was calibrated to be $S_{eff} = -(0.229 \pm 0.011)$ (fig. S4). We measured the spin polarization parallel to the sample normal and thus parallel to the initial electron velocity.

The spin polarization of photoelectrons from a clean Au(111) single crystal and the sign of its orientation depend on the laser polarization (Fig. 2A). An intensity asymmetry of $A = (5.03 \pm 1.1)\%$ was observed. Combined with the Sherman function S_{eff}, an electron spin polarization of $P = -(22 \pm 5)\%$ was determined for emission from